Yeast-to-hypha transition of *Schizosaccharomyces japonicus* in response to environmental stimuli

Cassandre Kinnaer, Omaya Dudin†, and Sophie G. Martin*
Department of Fundamental Microbiology, Faculty of Biology and Medicine, University of Lausanne, CH-1015 Lausanne, Switzerland

ABSTRACT **Many fungal species are dimorphic, exhibiting both unicellular yeast-like and filamentous forms. *Schizosaccharomyces japonicus*, a member of the fission yeast clade, is one such dimorphic fungus. Here, we first identify fruit extracts as natural, stress-free, starvation-independent inducers of filamentation, which we use to describe the properties of the dimorphic switch. During the yeast-to-hypha transition, the cell evolves from a bipolar to a unipolar system with 10-fold accelerated polarized growth but constant width, vacuoles segregated to the nongrowing half of the cell, and hyper-lengthening of the cell. We demonstrate unusual features of *S. japonicus* hyphae: these cells lack a Spitzenkörper, a vesicle distribution center at the hyphal tip, but display more rapid cytoskeleton-based transport than the yeast form, with actin cables being essential for the transition. *S. japonicus* hyphae also remain mononuclear and undergo complete cell divisions, which are highly asymmetric: one daughter cell inherits the vacuole, the other the growing tip. We show that these elongated cells scale their nuclear size, spindle length, and elongation rates, but display altered division size controls. This establishes *S. japonicus* as a unique system that switches between symmetric and asymmetric modes of growth and division.**

Monitoring Editor
Daniel J. Lew
Duke University

Received: Dec 6, 2018
Revised: Jan 31, 2019
Accepted: Feb 1, 2019

INTRODUCTION

Cellular morphologies are extremely varied. However, the overall mechanisms generating polarity are thought to be conserved across each species (Nelson, 2003). In fungi, whose shapes are defined by external rigid cell walls, the location of polarity factors on specific cortical regions drives cell growth locally through cell wall expansion and remodeling to generate specific cell morphologies. Many fungal species are dimorphic, exhibiting distinct morphologies depending on growth conditions. In this study, we used the fission yeast *Schizosaccharomyces japonicus*, a dimorphic species from the early-diverging ascomycete fission yeast clade, to describe the changes occurring during the dimorphic switch.

S. japonicus is estimated to have diverged 220 million years ago from its well-studied cousin *S. pombe*, with which it displays at least 85% orthologous genes (Rhind *et al.*, 2011). It can grow either in the yeast form, with dimensions slightly larger than those of *S. pombe*, or in a filamentous form (Niki, 2014). While fungal dimorphism is usually associated with pathogenicity (Nemecek *et al.*, 2006), *S. japonicus* is nonpathogenic to humans, making it a convenient model for the transition in growth mode. It was initially isolated on strawberries from a field in Japan in 1928 (Yukawa and Maki, 1931), and a variant was discovered more than a decade later by an American team in grape extracts (Wickerham and Duprat, 1945). The *S. japonicus* yeast form resembles that of *S. pombe*: cells are rod-shaped, divide medially, grow in a bipolar manner (Sipiczki *et al.*, 1998b), and use the small GTPase Cdc42 for cell morphology (Nozaki *et al.*, 2018). In *S. pombe*, Cdc42 controls cell shape by activating the formin For3 and the exocyst complex for polarized exocytosis of secretory vesicles (Martin and Arkowitz, 2014). However, it also displays important differences, notably in having semiopen mitosis (Yam *et al.*, 2011) and in division site positioning. In *S. pombe*,

This article was published online ahead of print in MBoC in Press (http://www.molbiolcell.org/cgi/doi/10.1091/mbc.E18-12-0774) on February 6, 2019.

Author contributions: C.K. and S.G.M. conceived the project; O.D. discovered the inducing action of fruit extracts and constructed the Pom1-GFP strain; C.K. performed all experiments; C.K. wrote the original draft; S.G.M. and C.K. edited it; S.G.M. obtained funding.

†Present address: Institut de Biologia Evolutiva (Consejo Superior de Investigaciones Cientificas—Universitat Pompeu Fabra), 08003 Barcelona, Spain.

*Address correspondence to: Sophie G. Martin (Sophie.Martin@unil.ch).

Abbreviations used: BE, blueberry extract; BF, brightfield; DIC, differential interference contrast; DMSO, dimethyl sulfoxide; DTT, dithiothreitol; EMM, Edinburgh minimal medium; LatA, latrunculin A; MBC, methyl benzimidazol-2-*yl*-carbamate; NLS, nuclear localization signal; RE, raspberry extract; RGE, red grape extract; SE, strawberry extract; WGE, white grape extract; YE, yeast extract.

septum positioning relies on positive signals from the nucleus, itself placed medially by associated microtubules pushing against both cell poles, and on negative signals preventing septum assembly at cell poles. The anillin-related protein Mid1 conveys the positive signal, whereas the DYRK-family kinase Pom1 serves to inhibit septation at cell poles (Sohrmann *et al*., 1996; Chang *et al*., 1997; Celton-Morizur *et al*., 2006; Padte *et al*., 2006; Huang *et al*., 2007). In *S. japonicus*, Pom1 kinase similarly controls medial division, but Mid1 is not required for division site placement (Gu *et al*., 2015).

The filamentous form of *S. japonicus* is triggered by environmental stresses (Sipiczki *et al*., 1998a), such as nutritional or nitrogen starvation, and DNA damage stresses (Furuya and Niki, 2010), suggesting that the switch from a small cell to a fast-growing hypha serves as a mechanism of escape from harsh environmental conditions. Filamentous growth is also light-repressed, as blue light perception by two *white-collar* light receptors present in *S. japonicus* and not in *S. pombe* induces hyphal cell division (Okamoto *et al*., 2013). Filamentous growth in *S. japonicus* is poorly characterized, though it is thought to share some traits common to other filamentous fungi, such as the presence of a large vacuole at the back of the cell (Sipiczki *et al*., 1998b).

Filamentous fungi, whether dimorphic (such as *Candida albicans* or *Ustilago maydis*) or not (such as *Neurospora crassa* or *Aspergillus nidulans*), grow through rapid apical extension mediated by a vesicle flux toward the growing tip (Riquelme, 2013). Polarized trafficking of vesicles provides the necessary membrane and wall-remodeling material to accommodate the rapid growth, from half to several micrometers per minute, of the filamentous form. Vesicles targeted for tip fusion typically accumulate in a spherical organelle, called the Spitzenkörper, which is located close to the growing tip and controls the hyphal growth rate and orientation (Riquelme and Sanchez-Leon, 2014). Lower fungi, such as Zygomycetes, and non-fungal Oomycetes do not require a Spitzenkörper to grow, but most other filamentous fungi assemble one, and it is generally described as a landmark of true filamentous growth (Grove and Bracker, 1970; Read *et al*., 2010). The hyphal forms of most filamentous fungi and dimorphic yeasts are multinuclear and their cytoplasm can be compartmentalized by septa that may be incomplete, maintaining cytosolic connection (reviewed in Steinberg *et al*., 2017). This contrasts with the yeast form, which is generally mononuclear and undergoes complete septal division, giving rise to a need for proper spatial coordination between mitosis and cytokinesis.

In this work, we describe the *S. japonicus* switch from yeast to hypha. We first identify fruit extracts as new inducers of hyphal formation that are independent of nutrient starvation. The *S. japonicus* hyphal form grows much faster and longer than the yeast form, but displays unique features amongst filamentous fungi. Indeed, it lacks a Spitzenkörper, undergoes complete cell divisions, and remains mononuclear. We find that cytoskeleton-based transport is more rapid in the hyphal than in the yeast form, with actin cables necessary for polarized growth, while microtubules contribute to nuclear positioning. *S. japonicus* hyphae divide asymmetrically: the front cell inherits a larger portion of the cytoplasm and no large vacuole, and exhibits altered size, growth, and division controls. Thus, the *S. japonicus* yeast-to-hypha transition involves the conversion of a symmetric to an asymmetric cell.

RESULTS

Fruit extracts induce filamentation in *Schizosaccharomyces japonicus*

Since *S. japonicus* was originally isolated from strawberries and grapes (Yukawa and Maki, 1931; Wickerham and Duprat, 1945), which may represent a natural habitat, we investigated whether these fruits alter the fungus growth behavior. Previous work established that induction of *S. japonicus* filamentation occurs upon stress by nutrient depletion and/or DNA damage (Aoki *et al*., 2017). On solid rich media in the absence of stress, *S. japonicus* primarily grows in the yeast form (Figure 1A). In contrast, within 3 d of growth on rich media plates supplemented with fruit extracts, *S. japonicus* colonies extended filaments at their periphery, appearing as a white halo around the yeast colony. The filamentation observed at colony edges was invasive, as it persisted after plate washing, indicating that the elongated cells had penetrated the solid media (Figure 1A). Invasive growth was observed with grape (red or white) and strawberry extracts, but also with other berry extracts. Filamentation was increased in the presence of higher concentration of red grape extract (RGE) and decreased with lower concentrations (Figure 1B). Note that in low-concentration RGE, filamentation was often observed only on parts of the colony's periphery, suggesting that the transition to the hyphal mode is a sporadic event under these conditions. In this work, we used 10% RGE to induce filamentation. RGE did not induce filamentation in other fission yeast species, nor in *Saccharomyces cerevisiae*, which can form pseudohyphae in certain conditions (Gimeno *et al*., 1992; Figure 1C). We note that the ability of RGE to induce filamentation on rich media suggests this is independent of nutrient stress, contrasting with previous reports associating filamentation with escape from stress (Sipiczki *et al*., 1998a; Furuya and Niki, 2010). This underlies the existence of different triggers and/or mechanisms by which *S. japonicus* transitions in growth forms. A tropism assay showed that *S. japonicus* filaments formed at least as much toward the RGE as away from it (Figure 1, D and E). Thus, although we cannot fully exclude oxidative stress as the trigger for the fruit extract–induced switch, this indicates that it is not a repellent. Initial characterization of the molecular properties of the RGE inducer showed that it is unlikely to be a nucleic acid, a protein, or a lipid and that it is heat-resistant. Phase separation with chloroform/methanol further determined that the inducer is water-soluble. However, the molecular identity of the inducer remains to be identified, as limited screening through candidate molecules present in fruit extracts, including glucose or fructose supplementation, has so far been unsuccessful (Table 1). In summary, fruit extracts represent new, likely stress-free, inducers for the switch to hyphal growth in *S. japonicus*.

The yeast-to-hypha transition involves extreme vacuolization and dramatic increase in cell size

Microscopy of hyphal cells growing on solid media proved to be challenging, due to the invasiveness of hyphae. Therefore, we performed imaging experiments in microfluidic chambers. In this setup, the cells are trapped between a flexible top layer made out of polydimethylsiloxane and a bottom glass layer, neither of which they can penetrate. Because blue light is inhibitory to filamentation (Okamoto *et al*., 2013), long-term microscopy was performed either with cells carrying a deletion of the white-collar light receptors Wcs1 and Wcs2 or in the presence of a blue-light filter. Under these growth conditions, we observed a progressive transition over 24 h to the filamentous form at the edges of microcolonies (Figure 2A; Supplemental Movie S1). Three successive stages in the transition from yeast to hypha can be described. The first landmark of filamentation is the appearance of multiple vacuoles all over the cytoplasm (Sipiczki *et al*., 1998b), forming a vacuolated yeast form. The vacuoles then polarized to one cell end in what we will refer as the transition form. Finally, once the vacuoles fused together into one or several large vacuoles, we refer to them as the hyphal form

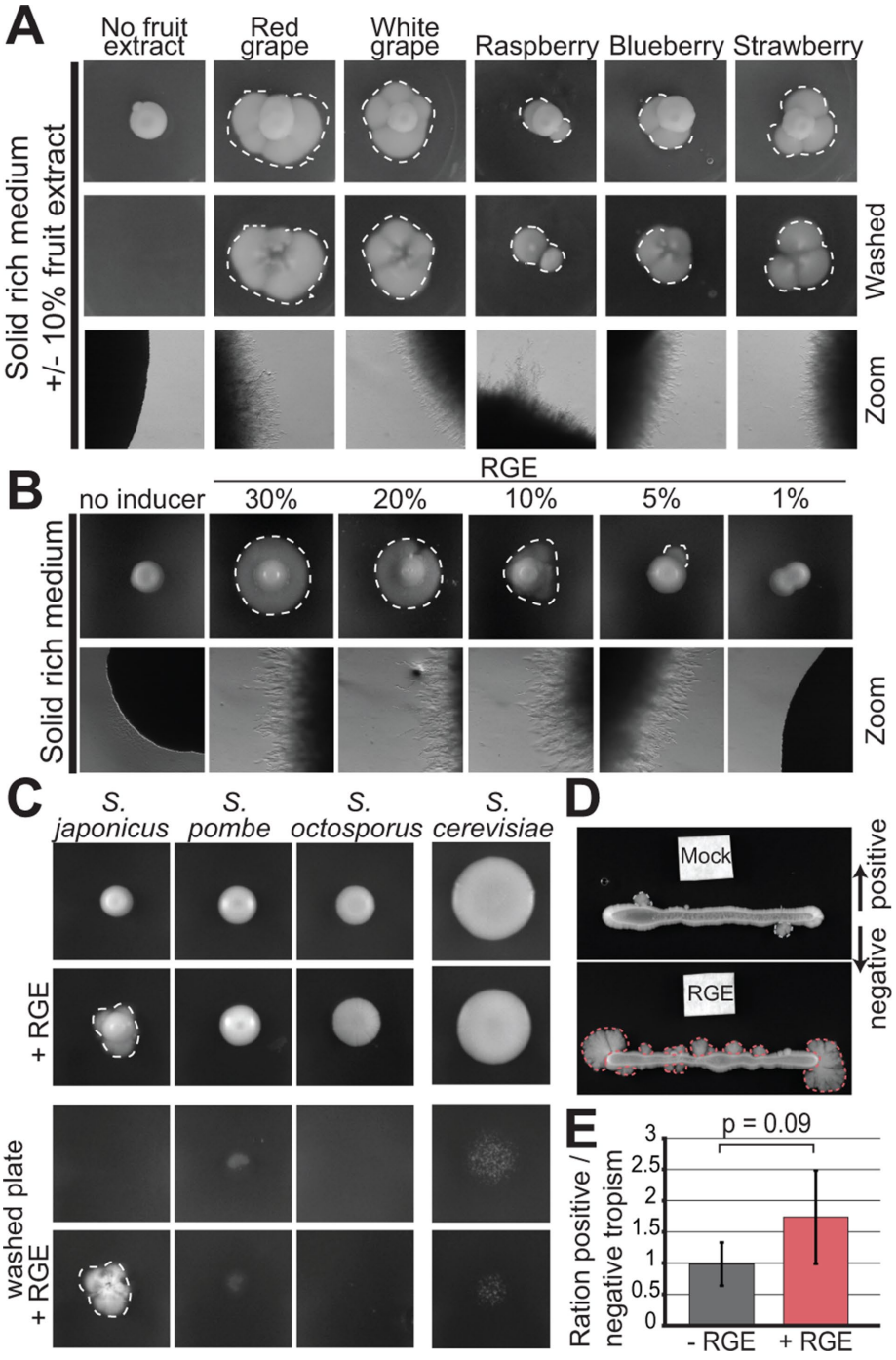

FIGURE 1: Fruit extracts induce invasive filamentation in *S. japonicus*. (A) *S. japonicus* growing in agar plates on solid rich media (YE), supplemented or not with 10% fruit extracts before (top) and after (middle) washing of the plate, as well as the same plates imaged under a stereomicroscope (bottom). (B) *S. japonicus* growing on solid rich media supplemented or not with a range of concentration of RGE and the same plates under the stereomicroscope. (C) *S. japonicus, S. pombe, S. octosporus*, and *S. cerevisiae* growing on solid rich media (YE or YPD) and supplemented or not with RGE before (top) and after (bottom) washing of the plate. (D) Tropism experiment to assess the directionality of *S. japonicus* hyphal growth. White filter squares were soaked with YE (top) or RGE (bottom). (E) Ratio of positive vs. negative growth tropism in experiments such as in D. Positive tropism denotes growth toward and negative tropism away from the filter; $p = 0.09$, *t* test. Error bars show standard deviations. Dotted lines highlight penetrative filamentous growth.

(Figure 2B). We confirmed that the organelles identified as vacuoles by DIC are indeed vacuoles, as these accumulate the water-soluble dye Lucifer yellow (Supplemental Figure S1). We also note that Lucifer yellow accumulates in smaller vacuoles present in the front of the hypha, which are difficult to detect by DIC. While the yeast and vacuolated yeast forms mainly grow in a bipolar manner, the transition and hyphal forms are always monopolar underlying a change in mode of growth (Figure 2C). In time course experiments, the earliest sign of vacuolization was observed 12 h after RGE induction, vacuole polarization at one end of the cell occurred after 18 h, and hyphae were observed 24 h after induction (Figure 2D). In the hyphal form, recognizable by its partitioning of the cytosol to the growing end of the cell and the vacuole to the back end, cell extension was strongly correlated with vacuole growth (Figure 2E). This suggests that the turgor pressure, which is an important driving force for growth, is supported by vacuole growth. Hyphae also grow about 10 times faster than the yeast form (Figure 2F). Indeed, hyphae extend at an average rate of 0.58 µm/min, whether RGE is added to rich or minimum medium, a rate comparable to that observed in other filamentous fungi, such as *C. albicans* and *A. nidulans*, which respectively grow at average rates of 0.76 and 0.5 µm/min (Gow and Gooday, 1982; Horio and Oakley, 2005). The monopolar transition form also displayed high growth rates, though slightly lower than hyphae (Figure 2F).

Schizosaccharomyces japonicus does not assemble a classical Spitzenkörper

In an effort to compare *S. japonicus* hyphae with those of other filamentous fungi and dimorphic yeasts, we looked for the presence of a Spitzenkörper at the hyphal tip. The accumulation of vesicles at the Spitzenkörper can be visualized in phase contrast microscopy as a dense spherical organelle (Riquelme and Sanchez-Leon, 2014) or fluorescently labeled with amphiphilic dyes such as FM4-64 (Fischer-Parton *et al.*, 2000) or with tagged Rab11 GTPase (Ypt3 in fission yeast), which decorates the vesicles (Cheng *et al.*, 2002). It can also be seen by the accumulation of type V myosin (Crampin *et al.*, 2005). In *S. japonicus*, neither phase contrast imaging nor FM4-64 showed a spherical signal at hyphal tips. Similarly, GFP-Ypt3 and Myo52-GFP did not reveal a spherical fluorescent signal, though they accumulated at the cortices of hyphal tips, consistent with local vesicle delivery at the site of growth (Figure 3A).

We further tagged other components of the polarization machinery: the exocyst component Exo70 and polarity proteins Bud6 and Spa2, thought to associate with formins, decorated the hyphal tip cortex; the microtubule-delivered Tea1 protein also assumed a localization similar to

	Yeast-to-hypha transition?	Conclusion
RGE treated with:		
Boiled	Yes	Inducer is not labile
RNase	Yes	Inducer is not RNA
DNase	Yes	Inducer is not DNA
Proteinase K	Yes	Inducer is not a protein
Chloroform	No	Inducer is not a lipid
MetOH	Yes (in soluble phase)	Inducer is a soluble component
Agar plate supplemented with:		
Red grape extract	+++	Inducer is in RGE
White grape extract	+++	Inducer is in WGE
Blueberry extract	+++	Inducer is in BE
Strawberry extract	+++	Inducer is in SE
Raspberry extract	+++	Inducer is in RE
Glucose	–	Inducer is not extra glucose
Fructose	–	Inducer is not fructose
Resveratrol	–	Inducer is not resveratrol
Ascorbic acid	–	Inducer is not ascorbic acid
Volatile chambers	–	Inducer is not a volatile
Ethanol	+	Small induction
Apple pectin	–	Inducer is not apple pectin
Aspartic acid	+	Small induction
Cellulose phosphate	+	
Gelatin	++	

TABLE 1: Hyphal inducing properties of fruit extracts and candidate molecules.

that described in the cousin species *S. pombe* (Figure 3B; Supplemental Movie S2; Takeshita *et al.*, 2008; Riquelme and Martinez-Nunez, 2016). None of these markers exhibited a Spitzenkörper-like localization. We conclude that *S. japonicus* does not assemble a classical Spitzenkörper like other filamentous fungi. Moreover, the localization of these polarity factors was similar in the hyphal and the yeast form, with the exception of Bud6, which decorated a notably wider region around the hyphal tip, and comparable to that of their homologues in *S. pombe* (Figure 3C). This suggests that the transition from yeast to hyphal form occurs without major reorganization of the polarity and trafficking machinery.

Actin-based trafficking is increased in the hyphal form and is essential for the transition

Although *S. japonicus* does not assemble a Spitzenkörper, live imaging of vesicles tagged with GFP-Ypt3 revealed an important change during the transition from yeast to hypha. Ypt3 vesicles accumulate at the growing tips in both the yeast and hyphal form of *S. japonicus* and their movement can also be tracked in the cytosol (Figure 4A; Supplemental Movies S3 and S4). Ypt3 fluorescence intensity was significantly increased at hyphal tips compared with that at yeast cell tips (Figure 4B), suggesting a greater accumulation of vesicles. This is likely to reflect an increase in membrane traffic to sustain the increase in cell growth. Interestingly, we found that the speed of individual vesicles was also on average significantly faster in hyphae than in yeast (Figure 4C). Similar fast vesicle speeds and accumulation at cell tips were also observed in the transition form, suggesting that the change in the rate of trafficking happens at the beginning of the transition.

Ypt3 trafficking occurred on F-actin, as actin depolymerization with LatA abolished all vesicle trafficking and cell tip localization (Cheng *et al.*, 2002; Figure 4, D and E; Supplemental Figure S2A). In contrast, microtubule depolymerization with MBC had no effect on Ypt3 trafficking. F-actin labeled with LifeAct-GFP was organized in actin patches, cables, and rings in *S. japonicus* (Alfa and Hyams, 1990). We noticed an accumulation of actin structures at the tips of growing hyphae coinciding with the increased growth rate for the hyphae (Figure 4F; see Figure 2F). Deletion of For3, the formin responsible for actin cable assembly in *S. pombe* (Feierbach and Chang, 2001), led to loss of actin cables in *S. japonicus*, as in *S. pombe*. However, the resulting mutant cells were sicker than their *S. pombe* counterparts (Feierbach and Chang, 2001; Bendezu and Martin, 2011), with impairment in growth and high cell mortality (Figure 4G; Supplemental Figure S2B). *for3*Δ mutant cells did not polarize growth, even in the presence of the inducer (Figure 4H). Thus, *S. japonicus* yeast and hyphal growth rely on transport of vesicles on actin cables for polarized growth, with increased rates of vesicular transport in the hyphal form.

Microtubules are dispensable for polarized growth of *S. japonicus*

We used GFP-Atb2 (alpha-tubulin) to examine the microtubule cytoskeleton. Microtubules form bundles aligned along the length of the cell in both yeast and hyphal forms (Alfa and Hyams, 1990; Sipiczki *et al.*, 1998b). In the yeast form, microtubule organization resembled that described in *S. pombe*, growing from cell middle toward cell ends, sliding along cell sides, and shrinking upon touching the cell tips (Figure 5A; Supplemental Movie S5). In the hyphal form, microtubule bundles were significantly longer, extending over the length of the cytoplasmic segment, and were often observed to bend (Figure 5A; Supplemental Movie S6). The bundles extended to the hyphal growing tip where they occasionally touched the membrane to deposit polarity factors (see Movie S2). Microtubules also extended through the vacuole-occupied cell segment, though rarely reached the other cell end (Figure 5B; see Figure 7E later in the paper). However, short-term microtubule depolymerization with MBC did not impair polarized growth in either yeast (unpublished data) or hyphal form (Figure 5C).

Because long-term MBC treatment during the yeast-to-hypha transition gave inconclusive results, likely due to effects on cell proliferation through disruption of the mitotic spindle, we assessed the role of microtubules during the transition by deleting the microtubule plus tip–associated CLIP-170 homologue Tip1. Though *tip1*Δ cells had some defects, notably in septum positioning, they retained the ability to polarize in the yeast form and to form hyphae within the same timeframe as wild type (Figure 5, D and E). Hyphae could also still penetrate the agar on solid medium (unpublished data). We conclude that microtubules and microtubule plus-tip factors are not important for the yeast-to-hypha transition or for hyphal growth.

Microtubule labeling also allowed us to visualize mitotic spindles, which elongated to significantly greater sizes in hyphae than

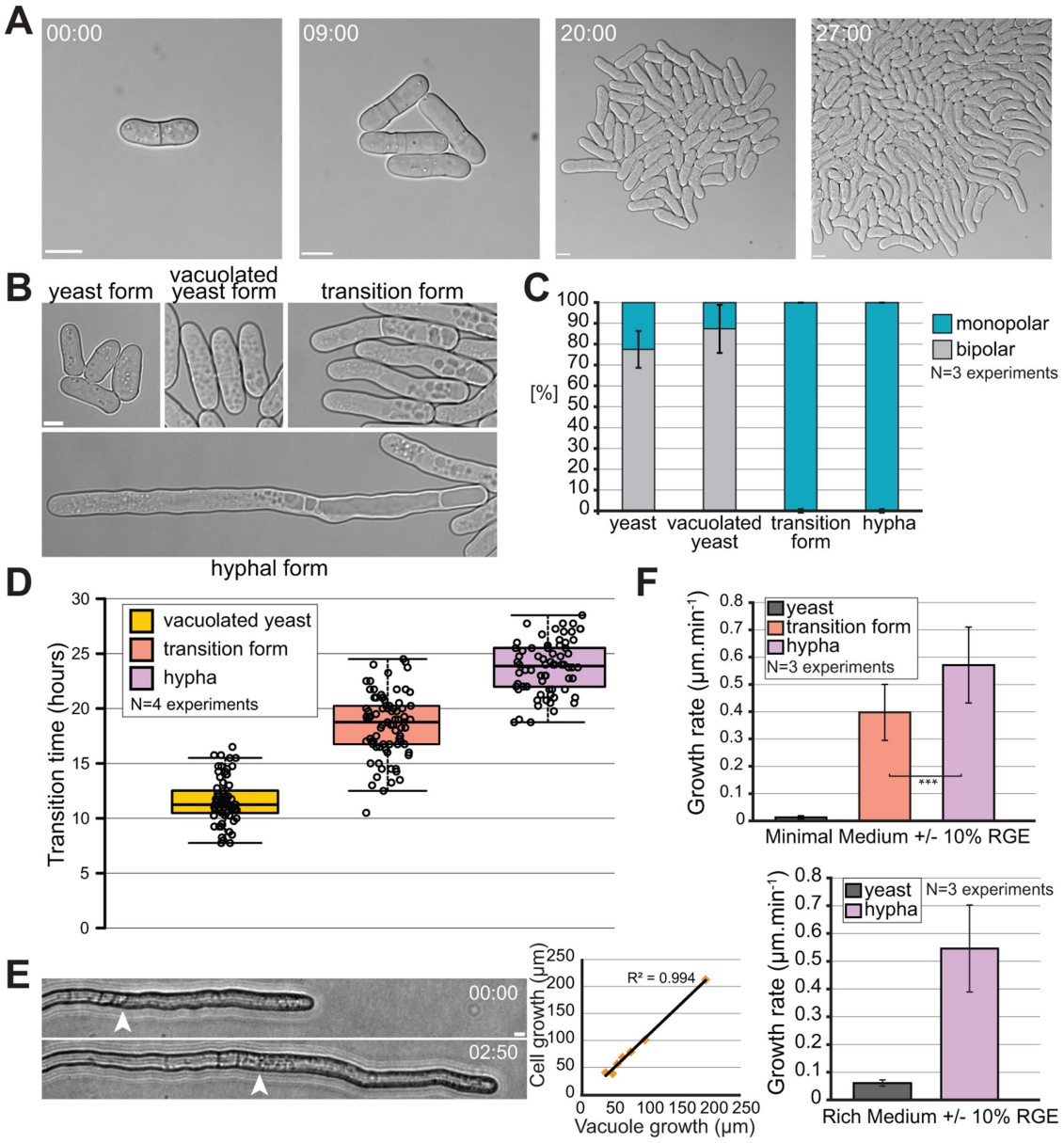

FIGURE 2: Kinetics of the morphological yeast-to-hypha transition. (A) DIC microscopy images of minicolony formation in a microfluidics chamber. (B) DIC microscopy images of the four identified morphological states of *S. japonicus* during the yeast-to-hypha transition in a microfluidic chamber. (C) Quantification of monopolar and bipolar cells in the four morphological states of *S. japonicus* ($n = 51$ hyphae and >100 cells for the other states). Yeast cells were quantified without RGE, the other forms 8–30 h after RGE addition. (D) Quantification showing time at which each morphological state first appeared after induction with RGE in microfluidic chambers ($n > 70$ cells per state). Box plot shows first and third quartile and median; whiskers extend 1.5 times the interquartile range from the first and third quartiles. (E) Bright-field microscopy images showing a growing hypha on solid medium (edge of vacuole shown with arrowhead) and quantification showing a correlation between the growth of the vacuole over time and the growth of an entire hypha over the same amount of time. $N = 7$ hyphae over five separate experiments. $R^2 = 0.994$, linear regression. (F) Quantification of the growth rates of different morphological forms on minimum and rich media (in minimal medium, $n = 60$ yeasts and >30 cells for the other states; in rich medium, $n = 60$ yeasts and 17 hyphae). Error bars show standard deviations. Time in h:min. Scale bars: 5 µm.

yeast cells: they reach over 30 µm in length, almost covering the entire cytosolic hyphal segment (Figure 5, F and G). Interestingly, the rate of spindle elongation was also significantly increased (~2.5-fold; Figure 5H), so that the total duration of mitosis tended to be even shorter in hyphae. We observed also less spindle buckling in hyphae (Yam *et al.*, 2011). This suggests that the rates of microtubule-dependent motors and thus dependent forces, similar to those of actin-dependent motors driving vesicle movements, are increased in hyphae.

Schizosaccharomyces japonicus hyphae display complete cell divisions and altered growth controls

We were surprised to observe that throughout the yeast-to-hypha transition, mitotic divisions were always followed by formation of

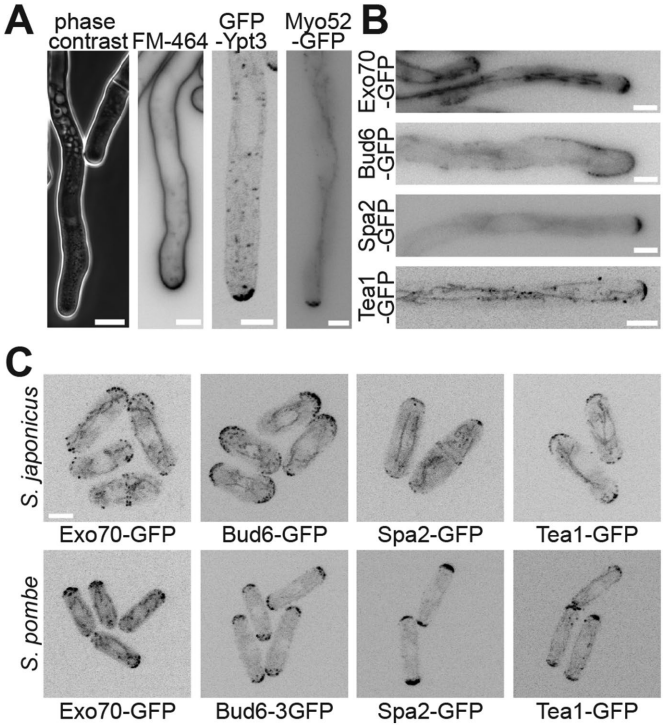

FIGURE 3: Localization of polarity factors in fission yeasts. (A) Hyphal tips of *S. japonicus* visualized with a phase contrast objective, stained with the amphiphilic dye FM4-64, marked with GFP-tagged Rab11 GTPase Ypt3 and expressing Myo52-GFP. Note that there is a slightly darker area at the tip of the hypha in the phase contrast image, but this is also present in the yeast form next to it, suggesting that it does not represent a Spitzenkörper. (B) Fluorescence images of GFP-tagged polarity proteins Exo70, Bud6, Spa2, and Tea1 at *S. japonicus* hyphal tips. (C) Fluorescence images of the same polarity proteins in *S. pombe* and *S. japonicus* yeast forms. Scale bars: 5 µm.

septa that constricted fully, giving rise to two daughter cells (Figure 6A; Supplemental Figure S3A). This was the case in cells lacking blue-light receptors as well as wild-type cells grown in the dark. Indeed, most filamentous fungi are multinucleated, with some forming septa that do not constrict but help compartmentalize an increasingly complex filamentous network (Mourino-Perez and Riquelme, 2013). Consistent with the completion of cytokinesis, *S. japonicus* remained mononuclear even in the filamentous form (Sipiczki *et al.*, 1998b; Figure 6, B and C). The nuclei were elongated in the hyphal form, with nuclear length correlating well with cytoplasm length, respecting the rule of constant nuclear-to-cytoplasmic ratio (Neumann and Nurse, 2007; Figure 6D). This observation, together with the absence of Spitzenkörper described above, sets *S. japonicus* hyphae apart from other filamentous fungi, casting them as more similar to the yeast form than expected.

Interestingly, in comparison to the yeast form, *S. japonicus* hyphae appeared to show distinct growth control. First, measurement of cell size at division showed an increase throughout the yeast-to-hypha transition, whereas cell width remained roughly constant, suggesting an alteration in cell size regulation during the transition (Figure 6E; Supplemental Figure S3B). This increase in size was not only due to the fast growth of the transition and hyphal forms, as the length of the cell cycle also increased (Figure 6F). Second, while *S. japonicus* yeast form and *S. pombe* stop growing during septation (Mitchison and Nurse, 1985), we found that the transition and hyphal forms continued to grow (Figure 6, G–I), similarly to what is observed in other filamentous fungi (Riquelme *et al.*, 2003). However, in these forms, the growth rate decreased during septation, interestingly by a similar absolute value, as in yeasts (Figure 6J). We envisage competition for polarity factors between the growing end and the septation site as a reason for this decrease.

Highly asymmetric cell division of a fission yeast in *Schizosaccharomyces japonicus*

One fascinating aspect of hyphal division is that this cell division is inherently highly asymmetric (Sipiczki *et al.*, 1998b). Indeed, hyphae (and transition forms) have polarized vacuoles to the back end of the cell and grow in a monopolar manner. Septation always occurred within the cytoplasm-containing cell segment. During cell division, one daughter cell retained the previously built vacuole and little cytosol and paused before growing a branch from the septation point. The other cell inherited most of the cytosol and the hyphal tip, which kept growing as described above. This cell rapidly rebuilt its vacuole close to the septation point (Figure 7A; Supplemental Movies S7 and S8). Similar behavior was observed in the transition form (Supplemental Figure S4). This raises the question of how hyphae position their division site.

We first investigated the mode of nuclear positioning. In *S. pombe*, the nucleus is positioned at mid-cell due to microtubules anchored at the nuclear envelope exerting pushing forces against both cell poles (Tran *et al.*, 2001; Daga *et al.*, 2006). In *S. japonicus* yeast cells, nuclei were at midcell, as in *S. pombe*. In contrast, in hyphae, nuclei were not at midcell, but were displaced toward the cell front because the vacuole occupies the back of the cell. However, they were also not centered within the cytosolic segment, but displaced toward the vacuole (Figure 7B). To examine the role of microtubules in nuclear positioning, we performed depolymerization experiments. In the yeast form, after more than 3 h of depolymerization with MBC, ~70% of the cells showed misplaced nuclei. After washout, most cells rapidly recentered their nuclei to the cell middle, indicating that microtubules control nuclear positioning (Figure 7C). A similar experiment in the hyphal form proved to be challenging, but examination of nuclear morphology during hyphal growth showed frequent nuclear shape deformation, indicative of forces exerted on the nuclear membrane (Figure 7D). Nuclear envelope deformations were seen on both sides of the nucleus, suggesting that microtubules exert forces from both sides. We noted above that microtubules penetrate the vacuole-occupied cell segment (see Figure 5B). The quantification of microtubule plus-end positioning within the cell showed a strong accumulation close to the hyphal tip, where according to data in *S. pombe*, they are expected to exert pushing forces. On the vacuole side, most microtubules were able to penetrate the space between the vacuole and the plasma membrane, though the majority ended within the first half of the vacuole length, suggesting that the pushing force may be partly dissipated (Figure 7E). Thus, we hypothesize that the force exerted on the nuclei by microtubules growing toward the vacuole is weaker than that produced by microtubules growing toward the hyphal tip, leading to the observed bias in nuclear positioning toward the vacuole.

Similarly to nuclei, hyphal septa were always positioned within the cytosolic cell segment, though they were off-centered toward the vacuole (Figure 7F). This position was unaltered in *mid1*Δ hyphae, indicating that, as in the yeast form (Gu *et al.*, 2015), Mid1 is not involved in septum positioning in *S. japonicus*. However, the predivisional nuclear position did not predict the septum position, which was better, though not perfectly, predicted by the middle of the anaphase spindle (Supplemental Figure S5). We note that, as in

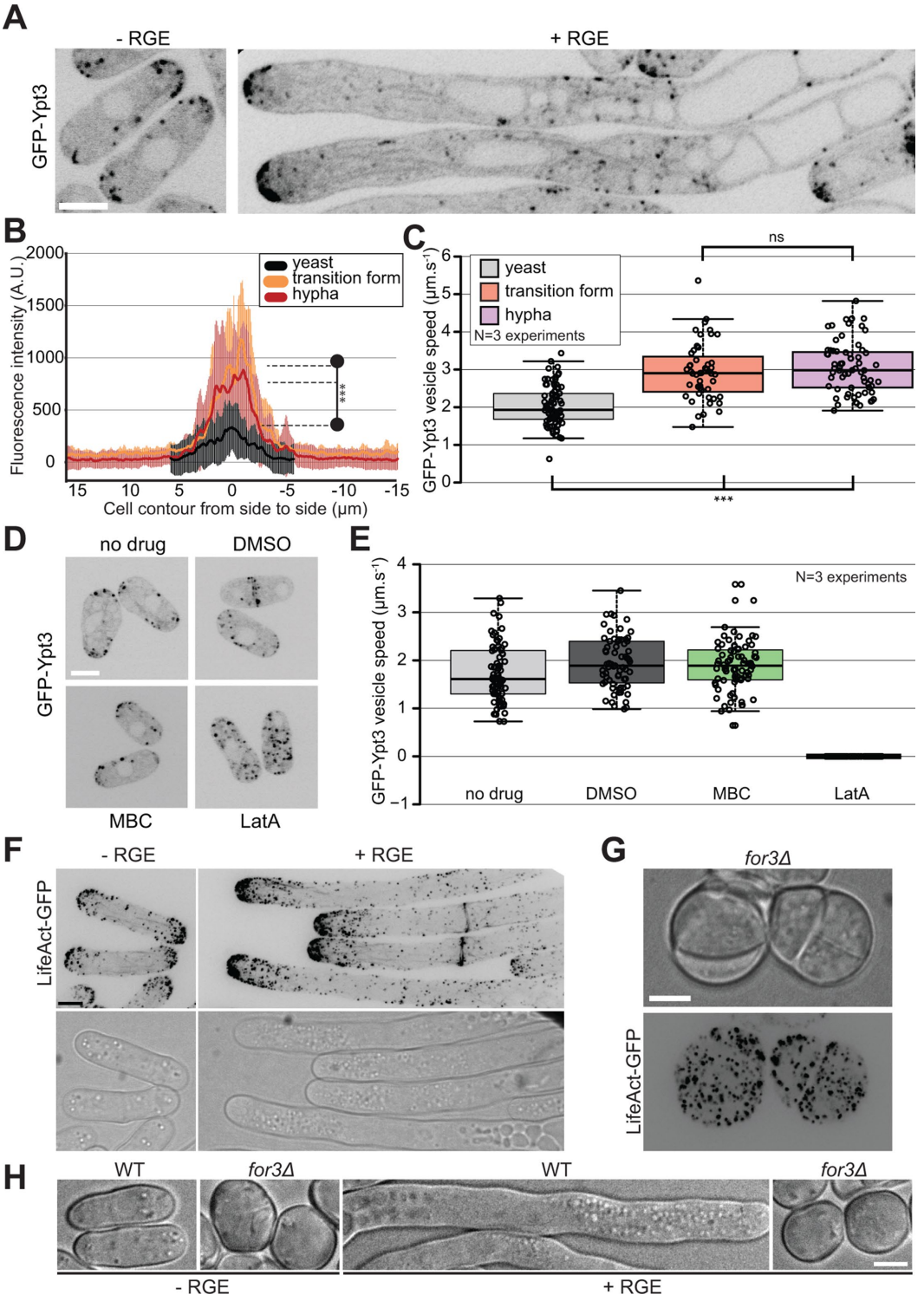

FIGURE 4: Actin-based trafficking is increased in the induced forms. (A) Middle-plane fluorescence images of *S. japonicus* cells expressing GFP-Ypt3 under both noninducing and inducing conditions. (B) Quantification of GFP-Ypt3 fluorescence intensity at the tips of yeasts ($n = 32$), transition forms ($n = 13$), and hyphae ($n = 18$). Shaded areas correspond to standard deviations. *** indicates $p < 1.2 \times 10^{-05}$; *t* test. (C) Quantification of vesicle trafficking speed in yeasts, transition forms, and hyphae. *** indicates $p < 4.82 \times 10^{-10}$; ns indicates $p = 0.44$; *t* test. (D) Middle-plane fluorescence images of GFP-Ypt3 in cells treated or not with solvent dimethyl sulfoxide (DMSO), microtubule-depolymerizing MBC, or actin-depolymerizing LatA. (E) Quantification of vesicle trafficking speed in cells treated as in D. (F) F-actin localization in *S. japonicus* observed with marker LifeAct-GFP in both yeast and hyphal forms. Images are maximum-intensity projections of 16 *z*-stacks (0.5 µm). (G) Fluorescence images of LifeAct-GFP in *for3*Δ mutants showing absence of actin cables and disorganized patches. (H) DIC images of wild-type and *for3*Δ mutants under noninducing and inducing conditions. Box plots show first and third quartile and median; whiskers extend 1.5 times the interquartile range from the first and third quartiles. Scale bars: 5 µm.

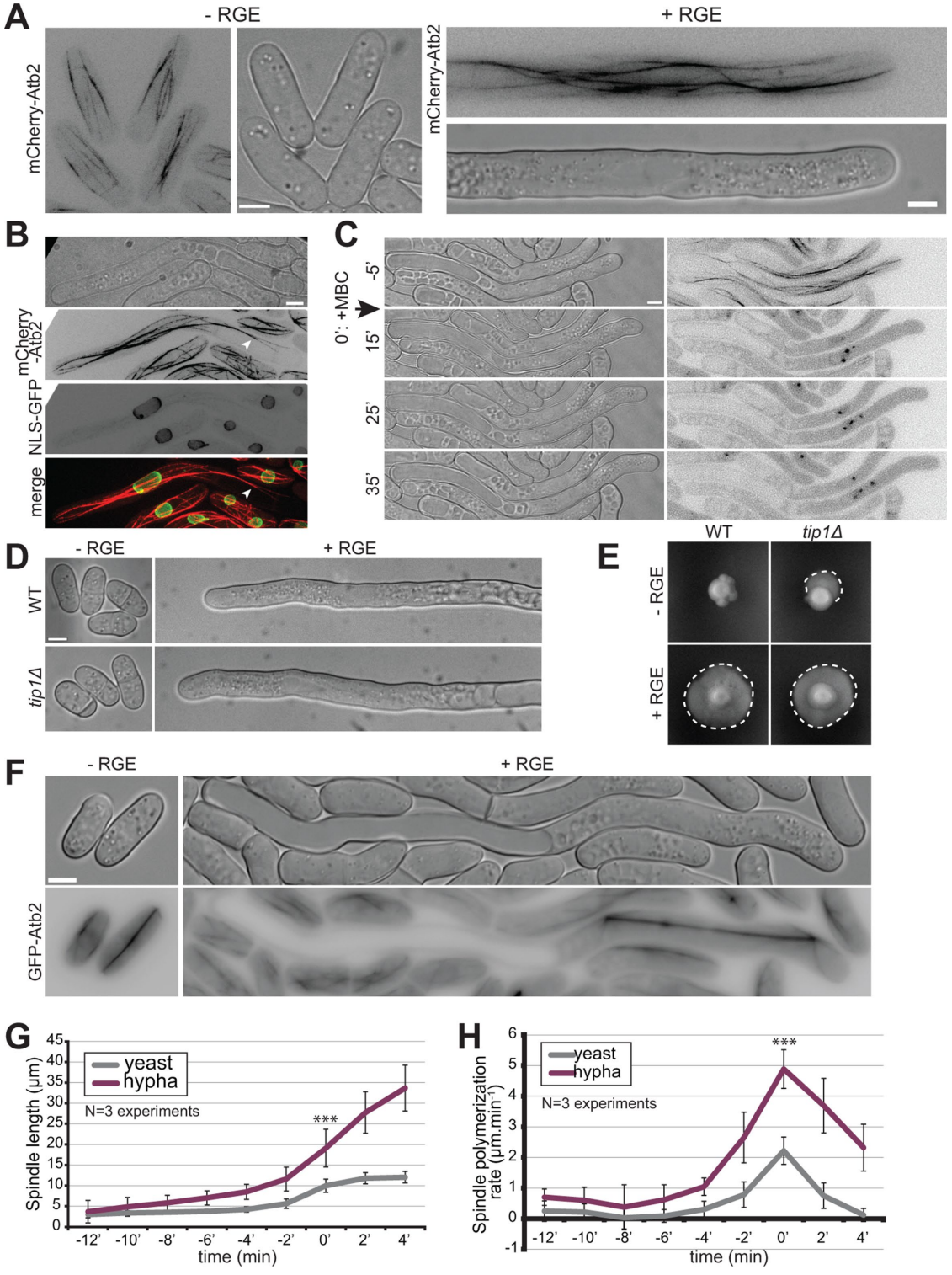

FIGURE 5: Microtubules are not involved in hyphal growth. (A) Microtubule organization in *S. japonicus* yeast and hyphal forms expressing mCherry-Atb2. Images are maximum-intensity projections of 8–14 *z*-stacks. (B) Images of an induced strain tagged with mCherry-Atb2 and NLS-GFP showing that microtubules can penetrate the space between the plasma membrane and the vacuole (arrowhead). (C) Microtubule depolymerization does not perturb hyphal growth. MBC was added at time 0 in a microfluidic chamber. (D) Wild-type and *tip1*Δ cells grown in microfluidic chambers under inducing and noninducing conditions. (E) Wild-type and *tip1*Δ strains grown on solid media under noninducing and inducing conditions. Dotted lines highlight penetrative filamentous growth. (F) Mitotic spindles labeled with GFP-Atb2 in yeast and hypha. (G) Quantification of spindle length over time, aligned on the steepest slope and averaged ($n = 30$ cells per cell type). (H) Quantification of spindle elongation rates over time. Individual profiles were aligned on the highest rate and averaged ($n = 30$ cells per cell type). *** indicates $p < 1.59 \times 10^{-10}$; *t* test. Error bars show standard deviations. Scale bars: 5 µm.

the yeast form, hyphal mitosis is semiopen (Supplemental Figure S5; Yam *et al.*, 2011). These observations suggest that positive signals for septum assembly may be conferred by the spindle.

Pom1 kinase constrains septum placement to midcell in *S. japonicus* yeast form, as it does in *S. pombe* (Gu *et al.*, 2015). Similarly, we found that *pom1*Δ hyphae showed septum mispositioning, where the septum was excessively displaced toward the vacuolar segment (Figure 7F). In *S. pombe*, this has been attributed to Pom1 gradients from cell poles exerting negative control to prevent septation at cell tips. A similar distribution is apparent in *S. japonicus* yeast cells (Figure 7G). Curiously, in hyphae, though Pom1-GFP accumulated at cell poles, it was also very distinctly present along cell sides, and it did not form an obvious long-range concentration gradient (Figure 7G). This raises the question of how Pom1 conveys positional information for septum placement.

DISCUSSION

A mycelium formed of single cells

It is believed that all Ascomycetes descend from a common filamentous ancestor (Berbee and Taylor, 1993). The fission yeasts form an early-diverging ascomycete clade, amongst which *S. japonicus* is the most divergent, suggesting that *S. japonicus* has retained an ancestral ability to filament present in the last common fission yeast ancestor (Sipiczki, 2000). In the fungal kingdom, filamentation leads to the formation of a mycelium, a complex multicellular network that underlies fungal spread and can reach several meters across (Smith *et al.*, 1992; Islam *et al.*, 2017). Mycelia are typically formed of a single, large common cytosol, which completely lacks septa in lower fungi, or is compartmentalized by incomplete, pore-containing septa in higher fungi (Steinberg *et al.*, 2017). As a result, mycelia can typically be considered as multinucleated syncytia. Hyphal fusion, or anastomosis, further increases the level of interconnectedness in fungi (Read *et al.*, 2009, 2010; Heaton *et al.*, 2012), and this plays an important role in nutrient exchange within a fungus (Simonin *et al.*, 2012). Although having a single cytoplasm extended over such lengths can appear risky, septate hyphae can easily seal off their septa, an absolutely vital process to prevent loss of cytoplasm in case of damage on the mycelium (Riquelme *et al.*, 2018), in case of an unfavorable environment (van Peer *et al.*, 2010), or during aging (Bleichrodt *et al.*, 2015). In this work we offer a description of a different kind of mycelium in *S. japonicus*.

The dimorphism observed in *S. japonicus* leads to the formation of extremely polarized and elongated single cells that are highly invasive of solid substrates, similarly to what is displayed by other filamentous organisms. In this work, we describe fruit extracts as novel inducers for the yeast-to-hypha transition in *S. japonicus*. Previously, nutrient starvation and DNA damage had been described as methods of induction of dimorphism in this fungus. Our method of induction appears to be specific for *S. japonicus*, as it did not trigger morphological transition in other fission yeasts or in *S. cerevisiae*, which forms penetrative pseudohyphae in response to nitrogen starvation (Gimeno *et al.*, 1992). We note that filamentous forms have been reported for *S. pombe* (Amoah-Buahin *et al.*, 2005), though RGE did not promote their formation. Cues triggering dimorphism are very varied in fungi; for example, *C. albicans* undergoes hyphal formation through a multitude of signals including serum and pH (reviewed in Sudbery, 2011), and *U. maydis* filamentation can be triggered by sexual pheromones and the resulting dikaryotic hyphae will infect maize plants (Nadal *et al.*, 2008). Interestingly, *S. japonicus* was isolated from both strawberries and grape extracts (Yukawa and Maki, 1931; Wickerham and Duprat, 1945), both of which we have shown to promote hyphal growth. This raises the question of its natural habitat and which morphological form it adopts in the wild. The hyphae produced by *S. japonicus* grow on the average at 0.58 μm·min^{-1}, a rate similar to what is observed in the true filamentous fungus *Aspergillus nidulans* (0.5 μm·min^{-1}; Horio and Oakley, 2005) and the fellow dimorphic yeast *C. albicans* (0.75 μm·min^{-1}; Gow and Gooday, 1982). Thus, in appearance, the transition of *S. japonicus* leads to the formation of a macroscopic mycelium.

However, in contrast to other mycelia, our study reveals that the *S. japonicus* mycelium is fragmented. Indeed, *S. japonicus* hyphae not only place septa, similar to what is observed in septate hyphae of higher fungi, but also divide fully after mitosis. As a result, all hyphae are mononuclear, an unusual feature for a filamentous organism. After hyphal division, both front and back cells resume growth, with the back one resuming growth at an angle behind the recently formed septum, which superficially resembles a branch point. However, we never observed true branching. The lack of a Spitzenkörper in *S. japonicus* hyphae is another point of divergence from other filamentous Ascomycetes. Indeed, the Spitzenkörper, a vesicle supply center that promotes and orients hyphal growth, is largely associated with Ascomycetes and Basidiomycetes septate hyphae, but is usually absent from early-diverging fungal lineages. Instead, we find that *S. japonicus* hyphae accumulate secretory vesicles at the growing tip in a less clustered pattern, similar to what was observed in yeast growth and filamentous Zygomycetes species (McClure *et al.*, 1968; Grove and Bracker, 1970; Roberson *et al.*, 2010). Finally, the strict dependence of hyphae on actin-based transport and independent from microtubules also cast it apart from many other filamentous fungi, which use microtubules for long-range transport (Egan *et al.*, 2012). These characteristics raise the question of whether the *S. japonicus* filamentous form should be considered true hyphae or pseudohyphae. Its complete septation and mononuclearity and its lack of Spitzenkörper are pseudohyphal characteristics. However, the very large vacuoles in *S. japonicus* filaments are a feature of hyphae. In many ways, except for the apparent absence of a Spitzenkörper, *S. japonicus* hyphae appears quite similar to those of *C. albicans*, which also form mononucleate compartments and rely on actin-based transport (Sudbery, 2011). Thus, the filamentation process of *S. japonicus* described here represents an intermediate form of filamentation and participates in the wide variety of filamentous forms in fungi.

Asymmetrical division in fission yeasts

An interesting aspect of the yeast-to-hypha transition in *S. japonicus* is the conversion of a symmetrical to an asymmetrical system. In the yeast form, the cell grows at both poles and divides in the middle, generating two apparently equivalent daughters, similarly to the case of *S. pombe*. In contrast, *S. japonicus* hyphae are morphologically and functionally very asymmetrical. Division yields a front cell that contains most of the cytoplasm and the unique growing tip and is shorter than the back cell, which is largely filled with an ever-growing vacuole and has to reinitiate growth with a delay. This asymmetrical conversion is already apparent early in the transition when cells switch to a monopolar mode of growth, which coincides with the accumulation of initially fragmented vacuoles at the back of the cell. Because *S. japonicus* can easily be induced to switch from a symmetrical to an asymmetrical division, the signals and mechanism of this conversion are rich grounds for future investigations.

One aspect we explored in a little more detail is the question of nuclear and septum positioning. While nucleus and septum are placed midcell in the yeast form, in wild-type hyphae we have shown that both are displaced away from the middle. The positioning

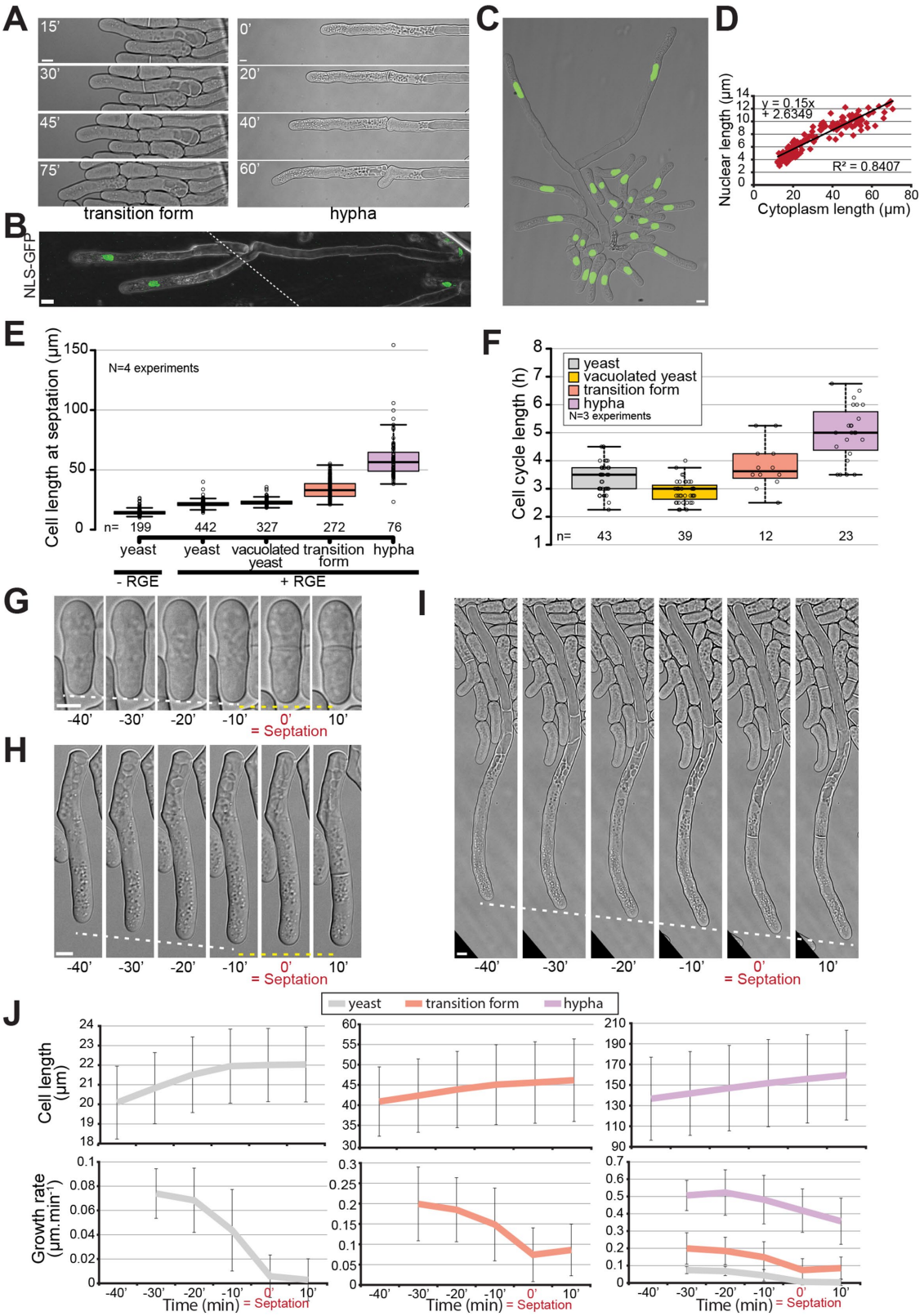

FIGURE 6: *S. japonicus* produces mononuclear hyphae. (A) DIC images of transition and hyphal forms showing completion of septation. (B) Tiled confocal microscopy image of hyphae expressing NLS-GFP growing on gelatin plates. Dotted line shows the location of the tiling. (C) Strain expressing NLS-GFP growing under inducing conditions in a microfluidics plate. (D) Correlation between nuclear length and cytoplasm length ($n = 178$ cells). (E) Quantification of cell length at septation in the different morphological forms of *S. japonicus*. (F) Quantification of cell cycle length in the different morphological forms of *S. japonicus*. (G–I) DIC images of cell growth in microfluidic plates up to the septation event. White dotted lines show tip growth. Yellow dotted lines show absence of or reduced growth. (J) Analysis of cell

mechanism for the nucleus can be inferred from work in *S. pombe*, which showed that microtubules anchored at the nuclear membrane exert pushing forces against cell poles, so that force balance is achieved when the nucleus is centered in the cell (Tran *et al.*, 2001; Daga *et al.*, 2006). Microtubules also exert forces for nuclear positioning in *S. japonicus*, as illustrated by the observations that decentered nuclei are recentered upon microtubule regrowth in yeast and the nuclear envelope is deformed by microtubules in hyphae. However, the nucleus is positioned neither in the middle of the hypha nor in the middle of the cytoplasmic region, but closer to the vacuole. We suggest that microtubule-dependent pushing forces position the nucleus, as in *S. pombe*, but that forces only become balanced at a nonmedial position due to force dispersion when microtubules encounter the vacuole at the back of the cell that is less rigid than the cell wall at the front.

The positioning of the septum is more mysterious. In *S. pombe*, septum positioning midcell is widely thought to rely on two complementary signals—a positive nuclear signal transmitted through the anillin-like protein Mid1, and a negative cell-pole signal dependent on Pom1 kinase (Sohrmann *et al.*, 1996; Chang *et al.*, 1997; Celton-Morizur *et al.*, 2006; Padte *et al.*, 2006; Huang *et al.*, 2007). In *S. japonicus* yeast cells, recent work showed that Mid1 plays no significant role in septum positioning (Gu *et al.*, 2015). We confirm this in hyphae, as septum position is not altered in *mid1*Δ cells. Consistently, we find that the septum position is poorly predicted by the predivisional nucleus, indicating that septum position is defined later than in *S. pombe*. The septum was closer to but not perfectly predicted by the center of the anaphase spindle, suggesting that positioning signals may be more similar to those used in metazoan cells, where the spindle is the key determinant (Oliferenko *et al.*, 2009). In contrast, Pom1 kinase regulates division site positioning in both yeast and hyphae (Gu *et al.*, 2015, and this work). For this function, Pom1 was proposed to form an inhibitory concentration gradient from the cell poles that counteracts the localization of medial cytokinetic node precursors, which in consequence preferentially form midcell (Celton-Morizur *et al.*, 2006; Padte *et al.*, 2006; Bhatia *et al.*, 2014; Rincon *et al.*, 2014). The long distance between the growing pole and the septum (over 50 µm on the average) calls this view into question, at least in hyphae. Indeed, although the Pom1-GFP distribution in yeast cells was very similar to that described for *S. pombe* (Hachet *et al.*, 2011), in hyphae it was only mildly enriched at tips and decorated most of the plasma membrane without forming an obvious long-range concentration gradient from the tip to the site of division. The cortex at the back of the cell, occupied by the vacuole, was also strongly decorated by Pom1, without enrichment at the back cell pole. This raises the question of how Pom1 conveys positional information for division in hyphae.

Size control

The *S. japonicus* yeast-to-hypha transition also provides an excellent system in which to study principles of size control. As the cell lengthens dramatically during the transition, several aspects of growth and division control are notably altered. *S. pombe* is arguably one of the best-studied systems for size control, due in part to its highly reproducible length at division. Measurements of cell size homeostasis concur in proposing that the system functions as a sizer (Wood and Nurse, 2015), with recent work suggesting that the key dimension for division timing is the surface area (Pan *et al.*, 2014). Whether this holds true for the *S. japonicus* yeast form is currently not known, but the much greater cell length of transition and hyphal cells at division indicates a profound change or relaxation in the mode of size control. Because cell cycle length is also increased during the transition, a simple timer model, where increased cell size would be acquired due to faster growth during a set time, is also unsatisfactory. However, we note that the often-observed correlation between cell and nuclear size (Jorgensen *et al.*, 2007; Neumann and Nurse, 2007; Webster *et al.*, 2009) is also present in *S. japonicus.* This correlation is spectacular, covering over sevenfold variation in size. The observed correlation occurs when nuclear size is compared with the cytoplasmic hyphal compartment rather than the whole cell, whose length varies according to the size of the vacuole. This is in agreement with data in *S. pombe* that support the idea that cytoplasmic volume determines nuclear size (Neumann and Nurse, 2007). These observations suggest that any size control in hyphae may monitor cytosolic and/or nuclear volume, excluding vacuoles, rather than length or surface area.

Many aspects of cell physiology are faster in the hyphae. First, polarized growth is over 10-fold faster, despite cell width remaining roughly constant. This indicates that the surface of the cell tip is not the limiting factor for polarized growth and that growth material must be supplied at an increased rate. Second, we find that secretory vesicles indeed display faster linear movements in hyphae. This increase in transport rate may contribute to, but is unlikely to fully explain, the increase in growth rate, because it is considerably smaller (~1.5-fold). However, it indicates that myosin (likely myosin V) motors inherently move faster, or are less impeded in their progression in the hypha. Third, it is intriguing that spindle elongation rates are similarly increased (~2.5-fold). As spindle elongation relies primarily on the action of kinesin motors, this suggests that kinesin motor speed is increased by a factor similar to that for myosin. As the duration of anaphase (as measured by the spindle elongation phase) is similar in yeast in hyphae, this produces much longer spindles in hyphae. Finally, we found that, in contrast to the yeast form, polar growth does not cease during hyphal division. In *S. pombe*, antagonism between two signaling pathways, the SIN and MOR pathways, is thought to control the alternation between cytokinesis and polarized growth (Ray *et al.*, 2010). This suggests that cross-talk between these two signaling pathways, and more generally between growth and division, is altered upon hyphal transition.

In summary, our detailed description of the yeast-to-hypha transition in *S. japonicus* provides founding work for addressing important fundamental cell biological questions. The identification of fruit extracts as an inducer permits a simple stress-free induction to study an important morphological transition. In particular, the conversion of the cell from a symmetrical to an asymmetrical division system and the massive changes in size in a single cell promise to reveal novel principles of division, growth, and size control.

MATERIALS AND METHODS

Strains and media

The original wild-type auxotrophic *S. japonicus* strains were kindly provided by H. Niki (National Institute of Genetics, Mishima, Japan)

length and growth rate over time aligned on septation time for yeast (gray), transition (orange), and hyphal (purple) forms ($n > 18$ cells per cell type). Box plots show first and third quartile and median; whiskers extend 1.5 times the interquartile range from the first and third quartiles. In J, error bars show standard deviations. Scale bars: 5 µm.

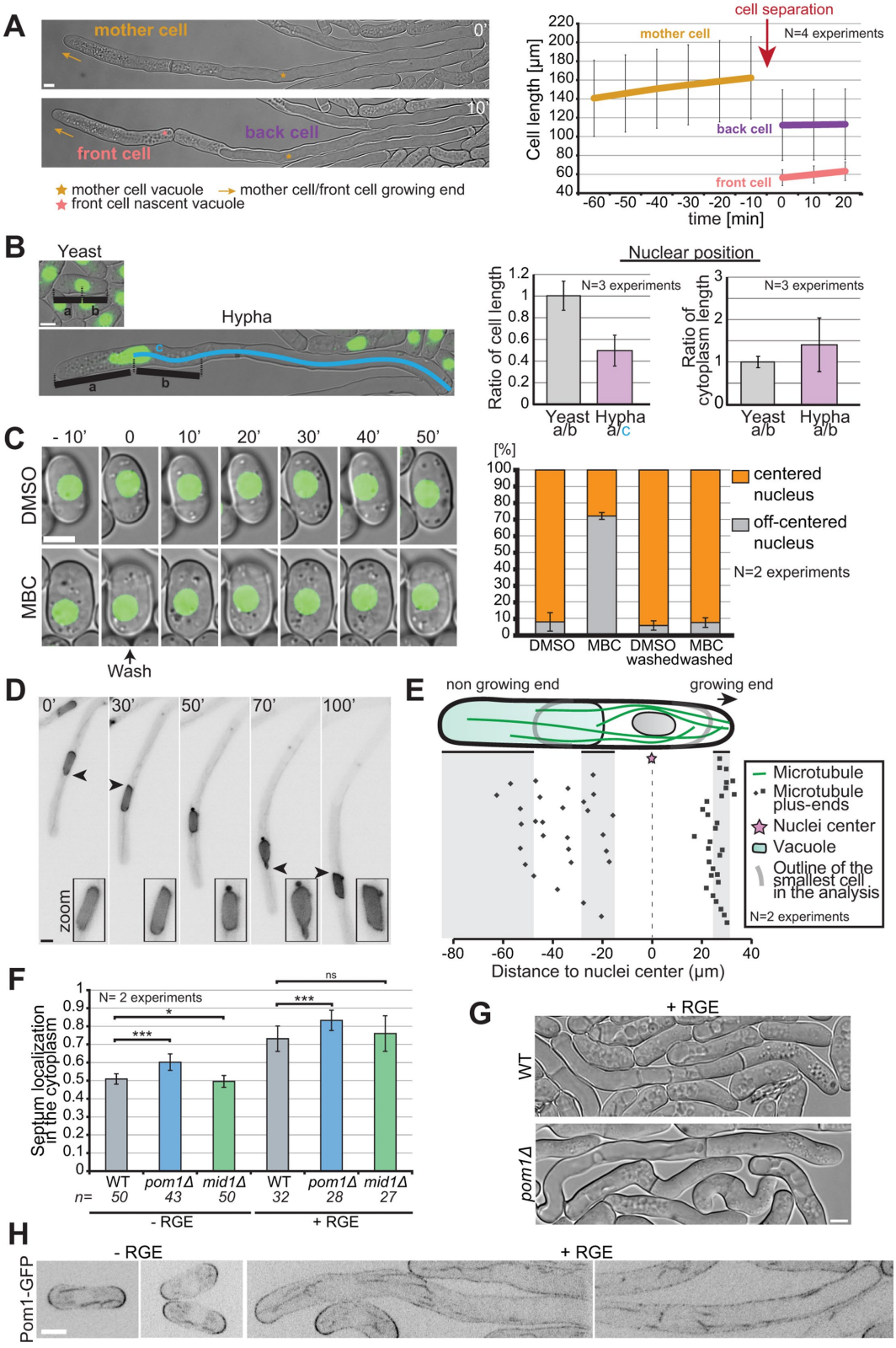

FIGURE 7: Asymmetric cell division in *S. japonicus*. (A) Hyphae divide asymmetrically, giving rise to a front cell that retains the growing end but has to rebuild a vacuole and a back cell that retains the vacuole but has to rebuild a growing end (left). Hyphal cell length recording over time aligned on cell separation (right) ($n = 20$ hyphae). (B) Quantification of nuclear positioning in the cell and in the cytoplasm. Positioning was calculated through ratios as explained in the left panel ($n > 50$ cells per cell type). (C) Microtubules contribute to nuclear positioning. Cells were grown in microfluidic chambers for 3 h with DMSO or MBC and then washed for 50 min with EMM-ALU. Nuclear position was quantified before and after the wash in >65 cells per condition. Note that most nuclei recentered rapidly after washout, but we quantified after 50 min to include a few delayed cells. (D) Fluorescence images of a hypha

(Furuya and Niki, 2009). The *S. japonicus* open reading frames (ORF) used in this study are the following: Atb2 (SJAG_02509), For3 (SJAG_04703), Spa2 (SJAG_03625.5), Bud6 (SJAG_04624.5), Tea1 (SJAG_01738), Exo70 (SJAG_04960), Ypt3 (SJAG_03915), Tip1 (SJAG_002695), Pom1 (SJAG_02392), Myo52 (SJAG_03011), Mid1 (SJAG_01143), Wcs1 (SJAG_02860), and Wcs2 (SJAG_05242). Cells were typically cultured in rich media (YE: yeast extract, 5 g; glucose, 30 g/l) for agar plate–based experiments and in Edinburgh minimal medium (EMM) supplemented with the appropriate amino acids (EMM-ALU) for microfluidic-based experiments. For plate experiments, 2 µl of a standardized cell concentration from a liquid preculture were deposited to form the initial colony. The fast growth of *S. japonicus* yeast cells in YE would entirely fill the microfluidic plates before transitioning to hyphae in presence of the inducer, which is why we chose to work with minimum media in this case. Red grape extract was obtained by blending 500 g of red grapes; the current batch of inducer was made from Crimson seedless grapes from Brazil. The blended grapes were placed in 50-ml Falcon tubes and centrifuged at 10,000 rpm for 25 min at room temperature (Eppendorf A-4-62). After recovery of the liquid supernatant by pipetting, the extract was placed in clean 50-ml tubes and centrifuged a second time (10,000 rpm, 15 min). Depending on the batch of grapes, this step was sometimes repeated. The grape extract was then filtered through a 0.22-µm filter (Millipore), aliquoted, and kept at –20°C for a maximum of 2 yr before degradation of the inducing capabilities. Hyphal formation was induced by adding 10% of RGE to liquid or solid media, unless otherwise stated. Crosses were done on SPAS media as previously described (Furuya and Niki, 2009) and strains were selected by random spore analysis.

S. pombe and *S. octosporus* cells were grown either on YE plates or, for imaging, in EMM-ALU. *S. cerevisiae* was grown on YPAD plates.

Strain construction in *Schizosaccharomyces japonicus*

The genome has been sequenced (Rhind *et al.*, 2011) and is available at http://fungidb.org/fungidb/. We used homologous recombination to introduce GFP or mCherry fluorescent markers or to delete a gene. Most of the plasmids constructed in this study were derived from pJK-210 backbone containing the ura4+ cassette from *S. japonicus*. This plasmid was constructed and kindly provided by S. Oliferenko (Crick Institute, London).

To create a gene deletion, the 5′ untranslated region (UTR) was linked with an inverted 3′ UTR fragment (1 kb each at least), separated by a unique restriction site, by PCR stitching and cloned in a ura4+-containing pJK210 plasmid. Homologous recombination in *S. japonicus* is only efficient when homology between the fragment to be integrated and the genomic locus extend to the very end of the fragment. We thus chose 3′ and 5′ UTR fragments in such a way that stitching reconstituted a blunt restriction enzyme site. Typically, we reconstructed a SmaI restriction site (CCCGGG) by choosing a 5′ UTR region to amplify that started with GGG and a 3′ UTR region that ended with CCC. Linearization of the plasmid and transformation led to gene replacement by the plasmid through homologous recombination.

To create Ypt3 fluorescently tagged N-terminally with GFP, the same procedure was used and the linked 3′ and 5′ UTR regions were inserted before the GFP coding sequence containing no stop codon. The ORF, with a stop codon, was inserted after the GFP and the plasmids were linearized with *Sma*I reconstructed between the stitched 3′ UTR and 5′ UTR regions.

To create an N-terminally tagged protein, mCherry-Atb2, we generated a plasmid containing the putative promoter of Atb2 (we amplified 1.4 kb upstream of the Atb2 ORF) followed by the mCherry coding region without the stop codon and the ORF of Atb2. This plasmid was linearized with *Afe*I located in the ura4 coding sequence on the plasmid and was transformed into a strain with a mutated *ura* locus, where it reconstructed a functional *ura* gene.

To create a protein tagged with a fluorescent marker at the C-terminus, we amplified at least 1 kb of the end of the ORF containing a restriction site and no stop codon and inserted it into the plasmid containing GFP or mCherry coding sequences. After linearization, the plasmid was transformed and inserted into the native loci of the genes of interest.

To mark the nuclei, we expressed GFP tagged with two nuclear localization signals using the promoter for Atb2 to drive the expression from the *ura* locus.

Transformation was done as previously described (Aoki *et al.*, 2010). Briefly, the cells were grown to the exponential phase and then washed in ice-cold water and 1 M sorbitol. After incubation with 1 M dithiothreitol (DTT), the cells were put in contact with at least 300 ng of linearized plasmid. Transformation of the cells was achieved through electroporation in 0.2-cm cuvettes, with the exact settings 2.3 KV, 200 Ω, 25 µF (Gene Pulser II; Biorad). Cells were left in liquid YE medium overnight to recover and plated the next day on selective media (EMM-AL, lacking uracil).

In the case of the construction of the Pom1-GFP strain, we linked together a fragment of the 3′ UTR region with a fragment of the end of the ORF without the stop codon and we cloned the stitched fragment in a pFA6a-GFP-kanMX plasmid in front of the fluorescent marker. After linearization, the plasmid was transformed in a wild-type prototroph strain following the same transformation protocol and selected on YE-G418 plates. All strains were checked for correct insertion of the plasmid with diagnostic PCR, and in the case of deletions, we also used primers inside the coding region and confirmed that the ORF was properly deleted.

Microscopy imaging

Wide-field microscopy was performed on a DeltaVision platform (Applied Precision) composed of a customized inverted microscope (IX-71; Olympus), a 60×/1.42 NA oil objective, a camera (CoolSNAP HQ2; Photometrics or PrimeBSI CMOS; Photometrics), and a color-combined unit illuminator (Insight SSI 7; Social Science Insights).

expressing NLS-GFP showing an example of nuclear shape alteration over time. Arrowheads point to nuclear envelope protrusion indicative of exerted forces. Insets show zoom on the nucleus. (E) Schematic of the localization of microtubule plus ends in the hyphal form. Each dot represents a microtubule plus-end position. The nuclear position was used as a reference point in all measurements. Shaded areas show the range of positions of the cell front, vacuole front, and cell back ($n = 50$ microtubule tips in 10 hyphae). (F) Quantification of septum position in the cytoplasm of yeast and hyphae, in WT, *pom1*Δ, and *mid1*Δ strains. ns: $p = 0.22$; *: $p = 0.03$; ***: $p < 9.08 \times 10^{-08}$; *t* test. (G) DIC images of septated WT and *pom1Δ* hyphae. Septation plane positioning in *pom1Δ* hyphae is biased toward the vacuole. (H) Middle plane fluorescence images of Pom1-GFP under inducing and noninducing conditions. In the hyphal form we show both the front and the back of cells. Scale bars: 5 µm.

Figures were acquired using softWoRx v4.1.2 software (Applied Precision). Spinning-disk microscopy was performed using an inverted microscope (DMI4000B; Leica) equipped with an HCX Plan Apochromat 100×/1.46 NA oil objective and an UltraVIEW system (PerkinElmer; including a real-time confocal scanning head [CSU22; Yokagawa Electric Corporation], solid-state laser lines, and an electron-multiplying charge-coupled device camera [C9100; Hamamatsu Photonics]). Stacks of *z*-series confocal sections were acquired at 0.5 to 1–μm intervals using Volocity software (PerkinElmer). Confocal microscopy tile scan images were acquired with a Zeiss laser scanning microscope (LSM 710) mounted with an EC Plan-Neofluar 40×/1.30NA oil objective. Images of growing yeast colonies on agar plates were imaged with a Leica MZ16 FA stereomicroscope (magnification 80–100×). Images of growing hyphae on agar pads were imaged with a Leica brightfield microscope mounted with a 20× air objective. Phase contrast imaging was acquired on Nikon Eclipse Ti microscope, mounted with a 100× phase contrast objective.

Hyphal transition experiments

A CellAsic ONIX microfluidics system was routinely used to image the transition (Millipore; Lee *et al.*, 2008). To image the yeast form, cells were grown overnight in 3 ml of liquid EMM-ALU to OD_{600} = 0.4 and then loaded into the plate 2 h prior to imaging to give them time to settle. To image the hyphal form, the cells were grown in liquid EMM-ALU overnight up to an OD_{600} of 0.1–0.2, loaded into the microfluidics plate, and grown in EMM-ALU-10%RG for 12–15 h before being imaged at 3 psi (20.7 kPa) in complete darkness (plate surrounded with aluminum foil) to induce hyphal formation. To observe the transition on solid agar plates (agar bacteriological, Oxoid, LP0011), we typically cultured *S. japonicus* overnight in 3 ml EMM-ALU and let the cells grow to the exponential phase. Cells were then spun down and concentrated before being plated on solid agar plates containing 10% of RGE. Hyphal growth was assessed 4–12 d later, as indicated. To assess growth rate in rich media, cells were grown on YE-2%agar microscopy pads supplemented or not with RGE for 12 h before imaging. For the confocal microscopy imaging, *S. japonicus* hyphae were grown on EMM-ALU 12% gelatin (Sigma-Aldrich; #48723) plates supplemented with 10% RGE for 8 d before a piece of gelatin containing hyphae was cut out and mounted on a slide for imaging.

Drug treatment and staining

To depolymerize actin, we used a 20-mM stock of Latrunculin A (LatA) dissolved in dimethyl sulfoxide (DMSO) to dilute exponentially growing cells to a final concentration of 200 μM. Methyl benzimidazole carbamate (MBC; Sigma) was used for the depolymerization of microtubules. A stock solution at 2.5 mg/ml in DMSO or ethanol was made fresh on the day of the experiment, and exponentially growing cells were treated at a final concentration of 25 μg/ml for 10 min at 30°C. To depolymerize microtubules in the microfluidics chambers, we flowed in EMM-ALU containing 25 μg/ml at 3 psi, which led to total depolymerization within 10–15 min, similar to the timing observed in liquid cultures. To wash the drug away, we flowed in EMM-ALU at 3 psi, and recovery of the cytoskeleton was observed within a few minutes. FM4-64 staining on growing hyphae was performed in microfluidics chambers as previously described (Fischer-Parton *et al.*, 2000). To label vacuoles with Lucifer yellow, cells were pregrown in EMM-ALU+10%RGE for 24 h at 25°C in the microfluidics device, incubated for 1 h with 4 mg/ml Lucifer yellow in water, and further washed for 1 h with EMM-ALU+RGE before imaging.

Treatment of red grape extract

To identify the molecule in the RGE responsible for the morphological transition, we subjected the RGE to a variety of physical and enzymatic treatments. RGE was treated with 16 U of proteinase K (New England Biolabs [NEB]; 800 U/ml), 20 and 100 U of DNase I (NEB; 2000 U/ml), and 1000 U of RNase If (NEB; 50,000 U/ml). RGE was heated to 95°C for 20 min. RGE was subjected to chloroform/methanol mix (1:1) and left to phase-separate overnight at –20°C. Both the resulting aqueous and organic phase were dried with a nitrogen stream and subsequently suspended in PBS 1X. All treated RGE were then included in solid agar plates and tested for hypha-inducing capabilities (see Table 1).

Supplementation of yeast extract media

To identify the molecule in the RGE responsible for the morphological transition, we also tried supplementing rich media with several likely molecular components of RGE and assess for hypha formation. Liquid YE media were individually supplemented with an additional 40 $g{\cdot}l^{-1}$ glucose, with 100 $g{\cdot}l^{-1}$ fructose, with concentrations ranging from 2 to 40 $mg{\cdot}l^{-1}$ resveratrol (Enzo Lifesciences),or with 270 $mg{\cdot}l^{-1}$ ascorbic acid. All supplemented YE media were then included in solid agar plates and tested for hypha-inducing capabilities (see Table 1).

Tropism assay

Cells were grown to exponential phase in YE and concentrated 10 times. On large Petri dishes (120 mm × 120 mm) containing YE–2% agar, we drew a 6-cm line in the middle of the plate on which 50 μl of cells was deposited. At 2 cm away from the center of the line, we dropped a small piece of chromatography paper (Whatman, 0.34 mm, #3030-917) onto which we pipetted 50 μl of RGE or YE (control). Plates were covered with aluminum foil and left at 30°C for 12 d before quantification of the area of hyphal growth. A ratio of positive tropism (growth toward the filter) on negative tropism (growth away from the filter) was calculated for both the experiment and the control plates for each plate and averaged over two experiments.

Identification of the different morphological forms

In all our experiments, we determined the stage of the morphological transition by looking at the polarity stage (monopolar/bipolar), the general localization of the vacuoles (all around the cytoplasm or already polarized at one pole), and the number of vacuoles:

Yeast: bipolar growth, no apparent vacuoles

Vacuolated yeast: bipolar growth, vacuoles all around the cytoplasm

Transition form: monopolar growth, many small vacuoles polarized at the nongrowing end

Hypha: monopolar growth, one or two larger vacuole(s) at the nongrowing end

Bipolar/monopolar quantification

In DIC (differential interference contrast) movies, we recorded how many cells had one or two poles growing in the different forms of the morphological transition.

Growth rate calculations

In DIC movies, we calculated the growth rate by measuring the change in cell or vacuole length over time. Cell growth rates on minimum media were calculated from cells growing on microfluidics

plates under inducing and noninducing conditions and were averaged over three experiments. Cell growth rates on rich media were calculated from cells growing on agar pads under inducing and noninducing conditions and were averaged over three experiments. The correlation of cell growth and vacuole growth was calculated from cells growing on agar pads under inducing conditions, each point in the graph representing a distinct hypha for which we calculated the extension length of the cell and the vacuole over the total time of the movies. We note that movies were of different lengths but clearly demonstrate the correlation between the two extension lengths.

Fluorescence levels

On spinning-disk medial focal planes of GFP-Ypt3–tagged cells (150 ms exposure, 100% laser power), we calculated the fluorescence intensity at the tips of yeasts and transitioning cells by drawing a segmented line 15 pixels in width around the cell periphery. We subtracted background noise averaged from two different fields of view per experiment. Fluorescence profiles were aligned with the geometric cell tip and averaged by cell type and over three experiments.

Quantification of vesicle speed

On spinning-disk movies, we manually measured the total trajectory of individual Ypt3 dots and derived the rate by dividing by the total time. Data were averaged over three experiments and averaged by cell type. Box plots were generated with http://shiny.chemgrid.org/boxplotr/.

Quantification of lengths

Spindle length was measured at each time point from appearance to complete elongation on epifluorescence movies of cells tagged with GFP-Atb2. Cell length was measured by drawing a line across the cell length from cell pole to cell pole on transmitted light images on septating cells. Box plots were generated with http://shiny.chemgrid.org/boxplotr/. Nuclear length was calculated by drawing a line across the nuclei tagged with NLS-GFP construct on epifluorescence images.

Cell cycle quantification

Cell cycle duration was quantified from septation event to septation event. On transmitted light movies containing the entire transition from yeast to hypha, we started our quantification by recording at what time the hypha septated at the end of the movie and then went "back in time" to the beginning of the movie following the lineage of the selected hypha and recording the time of each septation event in the lineage from final hypha to initial yeast. Results were averaged by cell type and over three experiments. Box plots were generated with http://shiny.chemgrid.org/boxplotr/.

Nuclear and septum positioning

To assess nuclear positioning in the cells, we measured the length from each cell tip to the middle of the nucleus on cells expressing NLS-GFP and plotted the two lengths as a ratio. For the induced forms, we plotted growing end length over nongrowing end length. Cells were averaged by cell type and over three experiments. To assess nuclear positioning in the cytoplasm in yeast, we used the same data as for nuclear positioning in the cell, as the entire cell length is filled with cytoplasm. To assess nuclear positioning in the cytoplasm in hyphae, we calculated the lengths from the growing cell tip to the middle of the nucleus and from the middle of the vacuolization zone to the middle of the nuclei. The vacuolization zone is the region in front of the large vacuole where small vacuoles are continuously delivered to the large one. We plotted the growing end length over the nongrowing end length. Results were averaged over three experiments. To assess septum positioning, we plotted the ratio of the length from the growing cell tips to the septum tor the length of the cytoplasm from transmitted light images. We averaged by cell type and over two experiments.

Quantification of microtubule plus-end localization

To measure microtubule plus-end positions in hyphae, we used the center of the nucleus as reference point and measured the distance to each microtubule plus end. Ten hyphae, with a total of 50 microtubules, were quantified. Microtubules pointing toward the growing tip have a positive distance value; those growing into the vacuolar compartment have a negative value. These distances were plotted on a graph, shown in Figure 7E. The accompanying schematic drawing indicates interval distances for the position of the vacuole and the two cell ends.

Microtubule-depolymerizing drug washing

In microfluidic chambers, we flowed cells with EMM-ALU supplemented with MBC (25 µg/ml final concentration) for 3 h before washing with EMM-ALU only. We assessed nuclear positioning in a strain expressing NLS-GFP before and after the wash. Even though microtubule repolymerization occurred in the first 10 min (unpublished data), we quantified the nuclear centering 50 min after the wash because some cells were slower to reposition their nuclei than others.

ACKNOWLEDGMENTS

We thank Snezhana Oliferenka (Crick Institute, London) for critical technical help at the start of the project. We thank her and Hironori Niki (National Institute of Genetics, Japan) for strains and reagents. This work was supported by EU Marie Curie Initial Training Network (ITN) FungiBrain funding and a Swiss National Science Foundation (SNF) grant (310030B_176396) to S.G.M. We are thankful to Serge Pelet and his group, as well as the Martin group, for critical reading of the manuscript.

REFERENCES

Alfa CE, Hyams JS (1990). Distribution of tubulin and actin through the cell division cycle of the fission yeast *Schizosaccharomyces japonicus* var. *versatilis*: a comparison with *Schizosaccharomyces pombe*. J Cell Sci 96 (Pt 1), 71–77.

Amoah-Buahin E, Bone N, Armstrong J (2005). Hyphal growth in the fission yeast *Schizosaccharomyces pombe*. Eukaryot Cell 4, 1287–1297.

Aoki K, Furuya K, Niki H (2017). *Schizosaccharomyces japonicus*: a distinct dimorphic yeast among the fission yeasts. Cold Spring Harb Protoc 2017, pdb top082651.

Aoki K, Nakajima R, Furuya K, Niki H (2010). Novel episomal vectors and a highly efficient transformation procedure for the fission yeast *Schizosaccharomyces japonicus*. Yeast 27, 1049–1060.

Bendezu FO, Martin SG (2011). Actin cables and the exocyst form two independent morphogenesis pathways in the fission yeast. Mol Biol Cell 22, 44–53.

Berbee ML, Taylor JW (1993). Dating the evolutionary radiations of the true fungi. Can J Bot 71, 1114–1127.

Bhatia P, Hachet O, Hersch M, Rincon SA, Berthelot-Grosjean M, Dalessi S, Basterra L, Bergmann S, Paoletti A, Martin SG (2014). Distinct levels in Pom1 gradients limit Cdr2 activity and localization to time and position division. Cell Cycle 13, 538–552.

Bleichrodt RJ, Hulsman M, Wosten HA, Reinders MJ (2015). Switching from a unicellular to multicellular organization in an *Aspergillus niger* hypha. mBio 6, e00111.

Celton-Morizur S, Racine V, Sibarita JB, Paoletti A (2006). Pom1 kinase links division plane position to cell polarity by regulating Mid1p cortical distribution. J Cell Sci 119, 4710–4718.
Chang F, Drubin D, Nurse P (1997). cdc12p, a protein required for cytokinesis in fission yeast, is a component of the cell division ring and interacts with profilin. J Cell Biol 137, 169–182.
Cheng H, Sugiura R, Wu W, Fujita M, Lu Y, Sio SO, Kawai R, Takegawa K, Shuntoh H, Kuno T (2002). Role of the Rab GTP-binding protein Ypt3 in the fission yeast exocytic pathway and its connection to calcineurin function. Mol Biol Cell 13, 2963–2976.
Crampin H, Finley K, Gerami-Nejad M, Court H, Gale C, Berman J, Sudbery P (2005). *Candida albicans* hyphae have a Spitzenkorper that is distinct from the polarisome found in yeast and pseudohyphae. J Cell Sci 118, 2935–2947.
Daga RR, Yonetani A, Chang F (2006). Asymmetric microtubule pushing forces in nuclear centering. Curr Biol 16, 1544–1550.
Egan MJ, McClintock MA, Reck-Peterson SL (2012). Microtubule-based transport in filamentous fungi. Curr Opin Microbiol 15, 637–645.
Feierbach B, Chang F (2001). Roles of the fission yeast formin for3p in cell polarity, actin cable formation and symmetric cell division. Curr Biol 11, 1656–1665.
Fischer-Parton S, Parton RM, Hickey PC, Dijksterhuis J, Atkinson HA, Read ND (2000). Confocal microscopy of FM4–64 as a tool for analysing endocytosis and vesicle trafficking in living fungal hyphae. J Microsc 198, 246–259.
Furuya K, Niki H (2009). Isolation of heterothallic haploid and auxotrophic mutants of *Schizosaccharomyces japonicus*. Yeast 26, 221–233.
Furuya K, Niki H (2010). The DNA damage checkpoint regulates a transition between yeast and hyphal growth in *Schizosaccharomyces japonicus*. Mol Cell Biol 30, 2909–2917.
Gimeno CJ, Ljungdahl PO, Styles CA, Fink GR (1992). Unipolar cell divisions in the yeast S. cerevisiae lead to filamentous growth: regulation by starvation and RAS. Cell 68, 1077–1090.
Gow NA, Gooday GW (1982). Growth kinetics and morphology of colonies of the filamentous form of *Candida albicans*. J Gen Microbiol 128, 2187–2194.
Grove SN, Bracker CE (1970). Protoplasmic organization of hyphal tips among fungi: vesicles and Spitzenkorper. J Bacteriol 104, 989–1009.
Gu Y, Yam C, Oliferenko S (2015). Rewiring of cellular division site selection in evolution of fission yeasts. Curr Biol 25, 1187–1194.
Hachet O, Berthelot-Grosjean M, Kokkoris K, Vincenzetti V, Moosbrugger J, Martin SG (2011). A phosphorylation cycle shapes gradients of the DYRK family kinase Pom1 at the plasma membrane. Cell 145, 1116–1128.
Heaton L, Obara B, Grau V, Jones N, Nakagaki T, Boddy L, Fricker MD (2012). Analysis of fungal networks. Fungal Biol Rev 26, 12–29.
Horio T, Oakley BR (2005). The role of microtubules in rapid hyphal tip growth of *Aspergillus nidulans*. Mol Biol Cell 16, 918–926.
Huang Y, Chew TG, Ge W, Balasubramanian MK (2007). Polarity determinants Tea1p, Tea4p, and Pom1p inhibit division-septum assembly at cell ends in fission yeast. Dev Cell 12, 987–996.
Islam MR, Tudryn G, Bucinell R, Schadler L, Picu RC (2017). Morphology and mechanics of fungal mycelium. Sci Rep 7, 13070.
Jorgensen P, Edgington NP, Schneider BL, Rupes I, Tyers M, Futcher B (2007). The size of the nucleus increases as yeast cells grow. Mol Biol Cell 18, 3523–3532.
Lee PJ, Helman NC, Lim WA, Hung PJ (2008). A microfluidic system for dynamic yeast cell imaging. BioTechniques 44, 91–95.
Martin SG, Arkowitz RA (2014). Cell polarization in budding and fission yeasts. FEMS Microbiol Rev 38, 228–253.
McClure WK, Park D, Robinson PM (1968). Apical organization in the somatic hyphae of fungi. J Gen Microbiol 50, 177–182.
Mitchison JM, Nurse P (1985). Growth in cell length in the fission yeast *Schizosaccharomyces pombe*. J Cell Sci 75, 357–376.
Mourino-Perez RR, Riquelme M (2013). Recent advances in septum biogenesis in *Neurospora crassa*. Adv Genet 83, 99–134.
Nadal M, Garcia-Pedrajas MD, Gold SE (2008). Dimorphism in fungal plant pathogens. FEMS Microbiol Lett 284, 127–134.
Nelson WJ (2003). Adaptation of core mechanisms to generate cell polarity. Nature 422, 766–774.
Nemecek JC, Wuthrich M, Klein BS (2006). Global control of dimorphism and virulence in fungi. Science 312, 583–588.
Neumann FR, Nurse P (2007). Nuclear size control in fission yeast. J Cell Biol 179, 593–600.
Niki H (2014). *Schizosaccharomyces japonicus*: the fission yeast is a fusion of yeast and hyphae. Yeast 31, 83–90.
Nozaki S, Furuya K, Niki H (2018). The Ras1-Cdc42 pathway is involved in hyphal development of *Schizosaccharomyces japonicus*. FEMS Yeast Res 18.
Okamoto S, Furuya K, Nozaki S, Aoki K, Niki H (2013). Synchronous activation of cell division by light or temperature stimuli in the dimorphic yeast *Schizosaccharomyces japonicus*. Eukaryot Cell 12, 1235–1243.
Oliferenko S, Chew TG, Balasubramanian MK (2009). Positioning cytokinesis. Genes Dev 23, 660–674.
Padte NN, Martin SG, Howard M, Chang F (2006). The cell-end factor pom1p inhibits mid1p in specification of the cell division plane in fission yeast. Curr Biol 16, 2480–2487.
Pan KZ, Saunders TE, Flor-Parra I, Howard M, Chang F (2014). Cortical regulation of cell size by a sizer cdr2p. eLife 3, e02040.
Ray S, Kume K, Gupta S, Ge W, Balasubramanian M, Hirata D, McCollum D (2010). The mitosis-to-interphase transition is coordinated by cross talk between the SIN and MOR pathways in *Schizosaccharomyces pombe*. J Cell Biol 190, 793–805.
Read ND, Fleißner A, Roca MG, Glass NL (2010). Hyphal fusion. In: Cellular and Molecular Biology of Filamentous Fungi, Washington, DC: American Society for Microbiology.
Read ND, Lichius A, Shoji JY, Goryachev AB (2009). Self-signalling and self-fusion in filamentous fungi. Curr Opin Microbiol 12, 608–615.
Rhind N, Chen Z, Yassour M, Thompson DA, Haas BJ, Habib N, Wapinski I, Roy S, Lin MF, Heiman DI, *et al*. (2011). Comparative functional genomics of the fission yeasts. Science 332, 930–936.
Rincon SA, Bhatia P, Bicho C, Guzman-Vendrell M, Fraisier V, Borek WE, Alves Fde L, Dingli F, Loew D, Rappsilber J, *et al*. (2014). Pom1 regulates the assembly of Cdr2-Mid1 cortical nodes for robust spatial control of cytokinesis. J Cell Biol 206, 61–77.
Riquelme M (2013). Tip growth in filamentous fungi: a road trip to the apex. Ann Rev Microbiol 67, 587–609.
Riquelme M, Aguirre J, Bartnicki-Garcia S, Braus GH, Feldbrugge M, Fleig U, Hansberg W, Herrera-Estrella A, Kamper J, Kuck U, *et al*. (2018). Fungal morphogenesis, from the polarized growth of hyphae to complex reproduction and infection structures. Microbiol Mol Biol Rev 82, doi: 10.1128/MMBR.00068-17.
Riquelme M, Fischer R, Bartnicki-Garcia S (2003). Apical growth and mitosis are independent processes in *Aspergillus nidulans*. Protoplasma 222, 211–215.
Riquelme M, Martinez-Nunez L (2016). Hyphal ontogeny in *Neurospora crassa*: a model organism for all seasons. F1000Research 5, 2801.
Riquelme M, Sanchez-Leon E (2014). The Spitzenkorper: a choreographer of fungal growth and morphogenesis. Curr Opin Microbiol 20, 27–33.
Roberson RW, Abril M, Blackwell M, Letcher P, McLaughlin DJ, Mouri ÑO-PÉrez RR, Riquelme M, Uchida M (2010). Hyphal structure. In: Cellular and Molecular Biology of Filamentous Fungi, Washington, DC: American Society for Microbiology.
Simonin A, Palma-Guerrero J, Fricker M, Glass NL (2012). Physiological significance of network organization in fungi. Eukaryot Cell 11, 1345–1352.
Sipiczki M (2000). Where does fission yeast sit on the tree of life? Genome Biol 1, REVIEWS1011.
Sipiczki M, Takeo K, Grallert A (1998b). Growth polarity transitions in a dimorphic fission yeast. Microbiology 144 (Pt 12), 3475–3485.
Sipiczki M, Takeo K, Yamaguchi M, Yoshida S, Miklos I (1998a). Environmentally controlled dimorphic cycle in a fission yeast. Microbiology 144 (Pt 5), 1319–1330.
Smith ML, Bruhn JN, Anderson JB (1992). The fungus *Armillaria bulbosa* is among the largest and oldest living organisms. Nature 356, 428.
Sohrmann M, Fankhauser C, Brodbeck C, Simanis V (1996). The dmf1/mid1 gene is essential for correct positioning of the division septum in fission yeast. Genes Dev 10, 2707–2719.
Steinberg G, Penalva MA, Riquelme M, Wosten HA, Harris SD (2017). Cell biology of hyphal growth. Microbiology Spectrum 5, doi: 10.1128/microbiolspec.FUNK-0034-2016.
Sudbery PE (2011). Growth of *Candida albicans* hyphae. Nat Rev Microbiol 9, 737–748.
Takeshita N, Higashitsuji Y, Konzack S, Fischer R (2008). Apical sterol-rich membranes are essential for localizing cell end markers that determine growth directionality in the filamentous fungus *Aspergillus nidulans*. Mol Biol Cell 19, 339–351.

Tran PT, Marsh L, Doye V, Inoue S, Chang F (2001). A mechanism for nuclear positioning in fission yeast based on microtubule pushing. J Cell Biol 153, 397–411.
van Peer AF, Wang F, van Driel KG, de Jong JF, van Donselaar EG, Muller WH, Boekhout T, Lugones LG, Wosten HA (2010). The septal pore cap is an organelle that functions in vegetative growth and mushroom formation of the wood-rot fungus *Schizophyllum commune*. Environ Microbiol 12, 833–844.
Webster M, Witkin KL, Cohen-Fix O (2009). Sizing up the nucleus: nuclear shape, size and nuclear-envelope assembly. J Cell Sci 122, 1477–1486.
Wickerham LJ, Duprat E (1945). A remarkable fission yeast, *Schizosaccharomyces versatilis* nov. sp. J Bacteriol 50, 597–607.
Wood E, Nurse P (2015). Sizing up to divide: mitotic cell-size control in fission yeast. Annu Rev Cell Dev Biol 31, 11–29.
Yam C, He Y, Zhang D, Chiam KH, Oliferenko S (2011). Divergent strategies for controlling the nuclear membrane satisfy geometric constraints during nuclear division. Curr Biol 21, 1314–1319.
Yukawa M, Maki T (1931). Regarding the new fission yeast *Schizosaccharomyces japonicus*. Kyushu Daigaku Kiyou [in Japanese], 218–226.